Orbital evolution and promotion effects in the photoionization dynamics of 2Σ− Rydberg states of OH

J. A. Stephens and V. McKoy

Citation: The Journal of Chemical Physics **93**, 7863 (1990); doi: 10.1063/1.459368
View online: http://dx.doi.org/10.1063/1.459368
View Table of Contents: http://scitation.aip.org/content/aip/journal/jcp/93/11?ver=pdfcov
Published by the AIP Publishing

Orbital evolution and promotion effects in the photoionization dynamics of $^2\Sigma^-$ Rydberg states of OH

J. A. Stephens and V. McKoy
Arthur Amos Noyes Laboratory of Chemical Physics,[a] *California Institute of Technology, Pasadena, California 91125*

(Received 16 July 1990; accepted 29 August 1990)

In this paper, we discuss the photoionization dynamics of the $D\,^2\Sigma^-(1\pi^2 3p\sigma)$ and $3\,^2\Sigma^-(1\pi^2 4s\sigma)$ Rydberg states of OH, emphasizing the critical role that Rydberg orbital evolution plays at intermediate to larger internuclear distances in determining vibrational and rotational molecular ion distributions. The orbital evolution process is discussed in terms of diabatic and adiabatic molecular states, united atom–separated atom correlation rules, and quantum defect functions. Vibrationally resolved photoelectron spectra and angular distributions for resonance enhanced multiphoton ionization (REMPI) of OH via the $D\,^2\Sigma^-(1\pi^2 5\sigma)$ and $3\,^2\Sigma^-(1\pi^2 6\sigma)$ Rydberg states are considered as examples. The results and conclusions are relevant to vibrationally and rotationally resolved REMPI studies of all first-row molecular hydrides, due to the similarity of their electronic structure and correspondence to their associated united atom.

I. INTRODUCTION

Presently there is interest in using resonance enhanced multiphoton ionization (REMPI) for the study and preparation of molecular ions with well-defined states of electronic, vibrational, and rotational energy. This goal, as well as obtaining basic understanding of the dynamical process, may be achieved through measurement of vibrationally and rotationally resolved ionic state branching ratios and photoelectron angular distributions.[1–5] The photoionization of molecular Rydberg states which are populated by resonant absorption of photons is generally expected to occur with the preservation of vibrational quantum numbers, due to the similarity of the neutral and ionic potential energy surfaces. Recently, mechanisms such as electronic autoionization of repulsive excited states[5–7] and shape-resonance-induced effects[5,8–12] have been shown to give rise to anomalous vibrational distributions in REMPI spectra. We recently discussed some results of studies of excited-state photoionization dynamics of the $D\,^2\Sigma^-(1\pi^2 3p\sigma)$ Rydberg state of OH.[13] The principal conclusion from this work was that the combination of conditions for a Cooper minimum and rapid changes in Rydberg orbital character at intermediate to larger internuclear distances may lead to significant non-Franck–Condon ion vibrational distributions.

The present paper discusses our earlier work[13] in a broader context, reports relevant calculational details, and presents calculations of vibrationally resolved photoelectron angular distributions for the $D\,^2\Sigma^-$ state. We discuss the orbital evolution processes associated with the Rydberg states in terms of diabatic and adiabatic molecular potentials, diabatic correlations between states of the united and separated atoms, and quantum defect functions as they depend on the internuclear separation. We also study the vibrational branching ratios and angular distributions for the next member of the Rydberg series converging to the $X\,^3\Sigma^-$ ion, the $3\,^2\Sigma^2(1\pi^2 4s\sigma)$ state.[14,15] The excited $4s\sigma$ orbital evolves in a manner "opposing" that of the $3p\sigma$ orbital of the $D\,^2\Sigma^-$ state, i.e., mainly into a $2p$ orbital on the hydrogen at moderate ($\sim 3a_0$) internuclear distances. These conditions lead to significantly *greater* Franck–Condon vibrational distributions, although due to a shift ($\sim 0.1a_0$) of the potential minimum to larger R relative to the $D\,^2\Sigma^-$ state, the vibrational distribution may be very broad. In the absence (or suppression) of the interactions mentioned above, we expect that REMPI via higher Rydberg states should result in Franck–Condon distributions obeying the $\Delta v = v^+ - v' = 0$ propensity rule, allowing in principle more efficient vibrational state selection.

An important dynamical feature of photoionization spectra relevant to the present studies are Cooper minima (or Cooper zeros) investigated theoretically initially by Bates[16] and Seaton[17] in the photoionization of the outer s subshell in the alkali atoms. Systematic studies and discussion of general rules for their occurrence for atoms was given by Cooper[18] and Fano and Cooper.[19] Cooper minima have also been identified and studied in the ground state of molecules with $3p$-type "lone-pair" orbitals.[20] Manson *et al.*[21,22] predicted and have systematically studied Cooper minima in the excited-state photoionization spectra of atoms whose characteristics may differ significantly from those observed from the ground state. For molecular excited states, very little is known. Fragmentary evidence of Cooper minima exist in the high-n discrete excitation spectra of NO and Na_2. Fredin *et al.*[23] have identified a Cooper minimum in the discrete spectra of NO utilizing optical–optical double resonance (OODR) techniques via the $C\,^2\Pi(3p\pi)$ state. Masnou-Seeuws and Jungen[24] have interpreted "fringes" in the OODR spectrum[25] of Na_2 as being due to Cooper minima in transitions from a $3p\sigma$ to high $ns\sigma$ and $nd\sigma$ Rydberg orbitals. Chupka has insightfully noted that Cooper minima may be particularly manifest in the excited-state photoionization spectra of the diatomic hydrides.[5] Our initial report focused on Rydberg orbital evolution and Cooper minimum in the

[a] Contribution No. 8172.

REMPI of OH,[13] in particular, the non-Franck–Condon effects which may be induced by their *combined* influence. These effects were predicted to be a common occurrence for REMPI dynamics of the first-row diatomic hydrides. The accompanying paper by Wang *et al.*[26] presents exploratory studies and predictions on the $3\,^3\Pi(1\pi 3p\sigma)$ state of the NH radical. In addition to vibrational distributions, the rapid evolution of the Rydberg orbital with internuclear distance in these systems has important implications for molecular ion rotational distributions. In particular, we have predicted that the rotational distribution of CH^+ for REMPI via the $E'\,^2\Sigma^+(3p\sigma)$ state should undergo complete inversion upon an increase of vibrational excitation of the intermediate state.[27] It has also been recently predicted that the Cooper minimum may be utilized to produce rotationally state-selected molecular ions in REMPI.[28,29]

Our initial theoretical studies have shown that changes in orbital form at intermediate to larger internuclear distances in the hydrides are particularly crucial in determining the nature of resulting vibrational and rotational ion distributions. In this regard, the REMPI technique coupled with photoelectron spectroscopy may provide a unique possibility to probe in detail the nature of the changes in the Rydberg molecular orbitals at larger R, in contrast to techniques which probe ionization directly from the molecular ground state.

II. CALCULATIONAL DETAILS

The calculation of vibrationally resolved cross sections and photoelectron angular distributions requires evaluation of the relevant photoionization transition moment over an appropriate range of photoelectron kinetic energies and internuclear distances. In the adiabatic-nuclei approximation, the cross section for photoionization of the v' level of the intermediate Rydberg state leading to the v^+ level of the ion is given by[30–32]

$$\sigma^{L,V}_{v^+\leftarrow v'} = \frac{4\pi^2 E}{3c}\sum_{lm\mu}|\langle\chi_{v^+}|I^{L,V}_{lm\mu}(R)|\chi_{v'}\rangle|^2. \tag{1}$$

$I^{L,V}_{lm\mu}$ are partial-wave components of the length (L) or velocity (V) incoming-wave normalized transition moment at internuclear separation R, defined as[33,34]

$$I^{L}_{lm\mu} = (k)^{1/2}\langle\Psi^{(-)}_{f,klm}|r_\mu|\Psi_i\rangle, \tag{2a}$$

$$I^{V}_{lm\mu} = \frac{(k)^{1/2}}{E}\langle\Psi^{(-)}_{f,klm}|\nabla_\mu|\Psi_i\rangle. \tag{2b}$$

In Eq. (1), E is the photon energy, c is the speed of light, and $\chi_{v'}$ and χ_{v^+} are the vibrational wave functions of the Rydberg and ionic states, respectively. In Eq. (2), Ψ_i is the resonant (Rydberg) state of the molecule with N bound electrons and Ψ_f is the final ionic state plus the photoelectron, and r_μ, ∇_μ ($\mu = 0, \pm 1$) are the components of the length and velocity form dipole operators in the body frame of the molecule.

For Ψ_i we use Hartree–Fock improved-virtual-orbital (IVO) wave functions[35] for the $D\,^2\Sigma^-(1\pi^2 3p\sigma)$ and $3\,^2\Sigma^-(1\pi^2 4s\sigma)$ Rydberg states. We used the Cartesian Gaussian basis set of our previous study[36] of ground-state photoionization of OH, augmented by diffuse s- and p-type Gaussian orbitals on the center-of-mass with exponents of 0.05, 0.03, 0.01, 0.005, and 0.001 for the Rydberg orbitals. In Table I, we give the calculated total energies [including the repulsive $1\,^2\Sigma^-(1\pi^2 3s\sigma)$ state] at various internuclear distances used in this study. For later discussion, in Table I we also give an angular momentum decomposition of the Rydberg orbitals according to the factor $N_{lm} = \int_0^\infty dr|\phi_{lm}(r)|^2$ ($m = 0$ for σ states, $m = \pm 1$ for π states), i.e., at all R we have the usual normalization for a bound orbital

$$\phi(\mathbf{r}) = \sum_{lm}\frac{\phi_{lm}(r)}{r}Y_{lm}(\hat{r}), \tag{3a}$$

$$\int d\mathbf{r}\,\phi^*(\mathbf{r})\phi(\mathbf{r}) = \sum_{lm}N_{lm} = 1. \tag{3b}$$

TABLE I. Total energies of OH $^2\Sigma^-$ Rydberg states and principal angular momentum composition of $n\sigma$ Rydberg orbitals, determined according to Eq. (3).[a]

$1\pi^2 4\sigma$	$1\pi^2 5\sigma$		$1\pi^2 6\sigma$				
R[b]	$-E_{\text{total}}$[b]	%s %p	$-E_{\text{total}}$	%s %p	$-E_{\text{total}}$	%s %p
1.200	74.8736	88.5 11.5	74.8138	12.1 87.8	74.7804	86.9 13.1
1.500	75.0923	86.2 13.4	75.0280	13.8 86.0	74.9970	85.3 14.6
1.834	75.1581	78.9 18.6	75.0868	22.1 77.1	75.0588	75.6 23.0
2.043	75.1684	68.3 23.7	75.0848	34.9 63.3	75.0619	54.3 42.7
2.250	75.1772	55.8 28.5	75.0735	57.8 38.1	75.0544	35.6 59.3
2.500	75.1911	44.0 29.4	75.0555	80.6 12.3	75.0372	11.9 85.8
3.000	75.2207	32.1 29.9	75.0164	86.4 5.3	74.9930	8.5 90.9
3.700	75.2494	23.9 26.1	74.9720	78.7 12.9	74.9423	15.9 84.0

[a] The calculated vertical excitation energy of the $^2\Sigma^-$ ($1\pi^2 5\sigma$) state from the $X\,^2\Pi$ ($1\pi^3$) ground state at $R_e = 1.8342a_0$ is 11.3 eV. The experimental value is 10.2 eV (Ref. 46). Beyond $\sim 2a_0$, the 4σ orbital loses contributions from the "3s" Rydberg state and has important contributions from $l = 2$ waves and higher (not shown, see discussion in the text).

[b] Internuclear distances and total energies are in atomic units.

For Ψ_f of Eq. (2), we employ the frozen-core approximation in which the bound orbitals of the ion are constrained to be identical to those of Ψ_i and the continuum photoelectron orbital hence satisfies a one-electron Schrödinger equation. This equation and the Coulomb and exchange coefficients for the $X\,^3\Sigma^-$ ion have been given in a ground state study of OH photoionization.[36] As discussed in Ref. 36, the photoelectron orbitals were obtained by the iterative Schwinger variational method, the details of which have been discussed in previous papers.[33,34] The basis sets used in the initial separable representation of the static-exchange potential

$$U \cong \sum_{i,j} \langle \mathbf{r}|U|\alpha_i\rangle (U^{-1})_{ij} \langle \alpha_j|U|\mathbf{r}'\rangle, \tag{4}$$

where the $|\alpha_i\rangle$ are chosen to be Cartesian Gaussian functions, are given in Table II.

Evaluation of Eq. (1) also requires accurate potential curves from which vibrational wave functions can be obtained. All vibrational wave functions were obtained by numerical integration. For the OH^+ $X\,^3\Sigma^-$ and OH $D\,^2\Sigma^-$ and $3\,^2\Sigma^-$ states, we used the *ab initio* potential curves of Werner *et al.*[37] and van Dishoeck *et al.*[15] As discussed in Sec. III, a complete set of vibrational distributions were also calculated using our IVO potential curve for the $3\,^2\Sigma^-$ $(1\pi^2 4s\sigma)$ state.

III. DISCUSSION

A. Orbital evolution processes in hydrides

1. Diabatic and adiabatic molecular states

The discussion and results in the following sections depend on changes in both the angular and radial nodal structures of the Rydberg molecular orbital with internuclear distance, a process we have operationally termed "orbital evolution." This encompasses electron promotion as well as changes in form of the orbital at intermediate ($\sim$2–3.5a_0) and larger R, due to "pseudocrossings" of the Rydberg adiabatic potential energy curves. To discuss the evolution process, it is convenient to point out relations between relevant diabatic (crossing) and adiabatic (noncrossing) potential energy curves, alternative representations of the Rydberg wave functions, and correlation rules which connect quantum numbers of the Rydberg electron in the united atom to those of the separated atoms (discussed below). The Rydberg wave function may be represented by the expansion

$$\Psi_{\alpha\sigma} = \sum_n C^{\alpha}_{n\sigma} A\,|\Phi_{\text{core}}\phi_{n\sigma}|, \tag{5}$$

where Φ_{core} represent the $N-1$ electrons of the ionic core, $\phi_{n\sigma}$ are members of a basis $\{\phi_{2p_0} - \phi_{H_{1s}}, \phi_{3s}, \phi_{3p}, \phi_{4s}, \phi_{4p}, \ldots\}$, and A represents antisymmetrization. Here the function $\phi_{2p_0} - \phi_{H_{1s}}$ represents the σ antibonding linear combination, while other terms represent the Rydberg basis wave functions whose electronic coordinate $\mathbf{r}$ is specified with respect to an atomic center. This representation of the Rydberg wave function is physically motivated by the close correspondence of the molecule to its united atom over a range extending beyond $R=0$, and likewise its rapid separation into atomic products over a range of R extending to 4 or $5a_0$. Note that the $\{|\Phi_{\text{core}}\phi_{n\sigma}|\}$ (diabatic) basis does not diagonalize the fixed-R electronic Hamiltonian and that Eq. (5) is identical in form, but not equivalent to that of an improved-virtual-orbital expansion, since the $\phi_{n\sigma}$ in Eq. (5) represent the unperturbed (but symmetry-adapted) states of the united or separated atoms at $R=0$ and $R=\infty$. The IVO orbital is obtained either from single-excitation configuration-interaction calculations within the subspace of (prediagonalized) virtual orbitals of σ symmetry,[38] or variationally as a solution of a one-electron eigenvalue equation.[35] Our single-center expansion parameters N_{lm} in Eq. (3) (and Table I) are expressed in terms of the expansion coefficients of Eq. (5) by

$$N_{lm} = \sum_{nl'} C^{\alpha}_{nl'} \int d\mathbf{r}\phi_{nl'}(\mathbf{r})\phi^*_{lm}(\mathbf{r}). \tag{6}$$

Note that the expansion parameters l' and l are defined with respect to the atomic centers and the center-of-mass, respectively. Given the known single-center expansion of the Ryd-

TABLE II. Basis sets used in the separable potential [Eq. (4)].

Photoionization symmetry	Center	Type of Gaussian function[a]	Exponents
σ	O	Cartesian s	8.0,4.0,2.0,1.0,0.5,0.1
		z	1.0,0.5,0.25,0.1
	H	Cartesian s	1.2,0.4,0.1,0.05
		z	1.2,0.4,0.1,0.05
	c.m.	Spherical $l=0$–3	2.0,1.0,0.5,0.1
π	O	Cartesian x	8.0,4.0,2.0,1.0,0.5,0.1,0.05
		xz	1.0,0.5,0.1,0.05
	H	Cartesian x	1.2,0.4,0.1,0.05
		xz	1.2,0.4,0.1,0.05
	c.m.	Spherical $l=1$–3	2.0,1.0,0.5,0.1

[a] Cartesian Gaussian basis functions are defined as $\phi^{\alpha,l,m,n\mathbf{A}}(\mathbf{r}) = N(x-A_x)^l(y-A_y)^m(z-A_z)^n \exp(-\alpha|\mathbf{r}-\mathbf{A}|^2)$ and spherical Gaussian functions are defined as $\phi^{\alpha,l,m\mathbf{A}}(\mathbf{r}) = N|\mathbf{r}-\mathbf{A}|^l \exp(-\alpha|\mathbf{r}-\mathbf{A}|^2) Y_{lm}(\Omega_{\mathbf{r}-\mathbf{A}})$. The Cartesian functions are centered on the nuclei and spherical functions are on the center-of-mass (c.m.).

berg orbital, i.e., Eq. (3a), one could determine directly the coefficients of Eq. (5) by matrix inversion, i.e., $\mathbf{C} = \mathbf{N} \cdot \mathbf{S}^{-1}$, where elements of the overlap matrix $\mathbf{S}$ are $S_{nl',lm} = \int d\mathbf{r}\, \phi_{nl'}(\mathbf{r}) \phi^*_{lm}(\mathbf{r})$. The corresponding diabatic potential energy at fixed R is given by the diagonal matrix element $E_d(R) = \langle \Phi_{\text{core}} \phi_{n\sigma} | H | \Phi_{\text{core}} \phi_{n\sigma} \rangle$. We have not evaluated explicitly the diabatic quantities, since analysis in terms of the N_{lm} is presently sufficient. Numerical procedures have been advanced to construct directly the diabatic molecular potentials, which may be of interest to apply in the present context.[39,40]

2. Diabatic correlation rules and pseudocrossings

Diabatic correlations between united atom and separated atom quantum numbers of diatomic molecules were discussed qualitatively very early by Weizel[41] and Mulliken,[42] and formulated theoretically for H_2^+ by Morse and Stückelberg.[43] For one-electron heteronuclear diatomics, these rules have also been rigorously derived by Gershtein and Krivchenkov.[44] For many-electron heteronuclear diatomics, these correlation rules have been discussed in the context of asymmetric atom–ion collisions (see particularly Fig. 5 of Ref. 45). This correlation conserves the radial quantum number $n_r = n - l - 1$, where n is the principal quantum number of the molecular orbital in the united and separated atom limits, either in the one-electron or many-electron system.[45]

In Fig. 1, we show diabatic correlations between the united atom and separated atom limits relevant to low-lying valence and Rydberg states of OH. In Fig. 2, we show adiabatic potential energy curves obtained directly from *ab initio* calculations[14,15,37] and qualitative diabatic potential curves (dashed lines) representing the united atom to separated atom correlation of Fig. 1. The potential minimum of the $D\,^2\Sigma^-$ state has been set at 10.2 eV, as determined by Douglas who first identified this state.[46] The atomic energy levels were obtained from the Moore compilation.[47] As the internuclear distance varies, pseudocrossings occur between the (diagonalized) adiabatic states $\Psi_{\alpha\sigma}$ with corresponding changes in the eigenvector components $C^{\alpha}_{n\sigma}$. That these pseudocrossings occur is enforced by requirements of the noncrossing rule of the adiabatic states $\Psi_{\alpha\sigma}$ and symmetry requirements given rigorously by the Wigner–Witmer symmetry rules.[48]

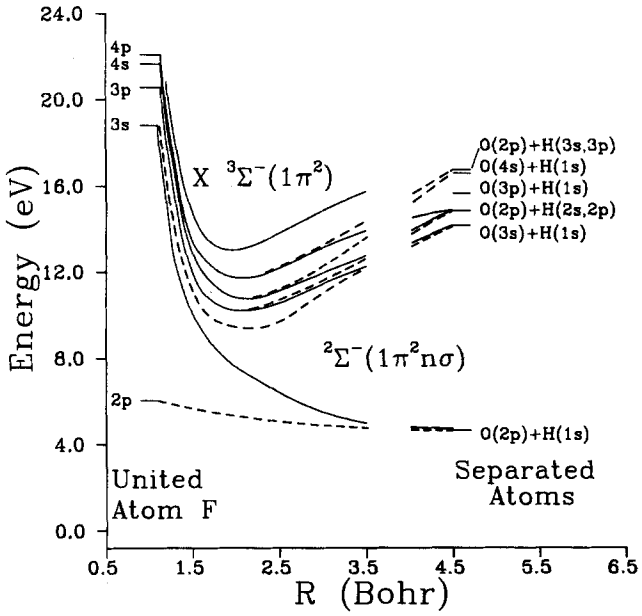

FIG. 2. Potential energy curves for the ground and first ionic states of OH and the excited states of the electronic configuration $^2\Sigma^-(1\pi^2 n\sigma)$ (from Refs. 15 and 37). The fluorine and oxygen atomic energy levels are from Ref. 47. The quasidiabatic potential curves are indicated by the dashed lines.

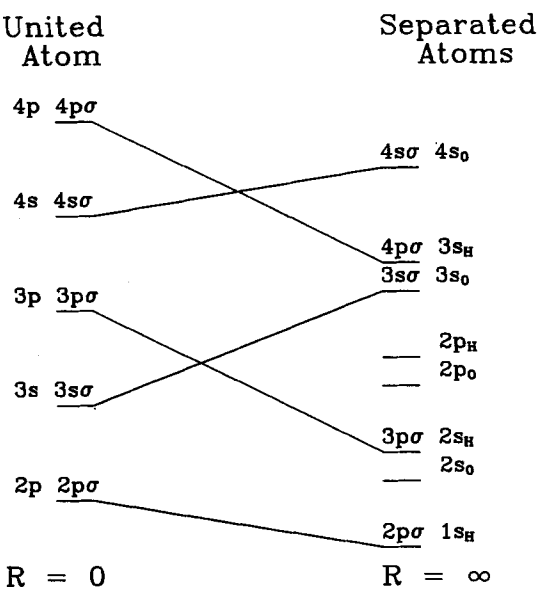

FIG. 1. The correlation diagram between the united atom orbitals of fluorine and separated atom orbitals of oxygen and hydrogen (see the text for discussion).

Figure 1 states that promotion of a $1s$ orbital on hydrogen at $R = \infty$ to a $2p$ orbital in the united atom must occur, as is well known in H_2. Likewise, the $3p\sigma$ and $4p\sigma$ levels can be considered promoted from $2s$ and $3s$ hydrogen orbitals at large R. These promoted levels, however, cross lower atomic levels of the united atom in the diabatic representation. In the adiabatic picture, the residual Coulomb interactions represented by the matrix elements in the diabatic basis $\langle \Phi_{\text{core}} \phi_{n\sigma} | H | \Phi_{\text{core}} \phi_{n'\sigma} \rangle$ are *large* essentially *everywhere* beyond $R \sim 0$, due to the mutual proximity of the united atom Rydberg levels n for $R > 0$ and the noncentral ionic core, which mixes Rydberg states with different l. That is, "localized" avoided crossings are not apparent in the adiabatic potential curves in Fig. 2 and the residual Coulomb interactions essential in the present context are accounted for by the one-electron, Hartree–Fock-IVO procedure. The residual Coulomb interactions and requirement of noncrossing therefore enforces a change in the number of radial nodes in the Rydberg wave function as R varies. For example, the 5σ orbital evolves as "$3p\sigma$" (one radial node) to "$3s\sigma$" (two radial nodes), as reflected in Table I, and verified by examining the radial wave functions. At larger $R(> 3a_0)$ for the 5σ

orbital, the mixing with the oxygen and hydrogen $2p$ orbitals is also apparent from Table I. These critical changes govern essential aspects of the photoionization dynamics from these Rydberg levels (non-Franck–Condon and Cooper minimum effects) as discussed in Sec. III B.

3. Variation of quantum defect functions with R

The basic connection among electron promotion, orbital evolution, and the global behavior of the quantum defect function with changing nuclear coordinates has been recognized,[49] particularly in regard to the $^1\Sigma_u^+(1\sigma_g np\sigma_u)$ Rydberg states of H_2. The quantum defect functions $\mu_{n\Sigma}(R)$ for Rydberg states of Σ symmetry are defined through the Rydberg equation (in a.u.)

$$U_{n\Sigma}(R) = U^+(R) - \frac{1}{2[n-\mu_{n\Sigma}(R)]^2},$$

where $U_{n\Sigma}(R)$ is the potential energy of the neutral Rydberg state and $U^+(R)$ is the potential energy of the ion. In Fig. 3, we show our calculated (static-exchange) quantum defect functions as a function of the internuclear distance considered in this work, for the OH $^2\Sigma^-$ (4σ–7σ) Rydberg states. Their variation reflects basic changes in forms of the Rydberg orbitals with R and also affords a somewhat limited comparison with the quantum defect functions of the $n\Sigma$ states of H_2 (see Fig. 2 of Ref. 49). In Fig. 3, we see that from $R \sim 1.0$–$1.8a_0$, the 4σ–7σ levels have quantum defects corresponding closely to the united atom, e.g., $\mu \sim 1.2$ and 0.7 for ns and np states, respectively. From $R \sim 1.8$–$3.0a_0$, all orbitals change their form most rapidly, as reflected in Table I and the quantum defects of Fig. 3. There the 4σ quantum defect rises through ~ 0.75. A complete change of unity reflects almost a pure promotional effect as in the $^1\Sigma_u^+(1\sigma_g 1\sigma_u)$ state H_2.[49] The quantum defect of the next ns series member, the 6σ level, rises as R increases due to its strong mixing with the adjoint 5σ level [note that the $4s$ diabatic curve would cross the O($3p$) level at larger R], but a pseudocrossing in the range ~ 2.5–$3.0a_0$ forces its decrease towards the H($2p$) level in the separated atom. The 5σ and 7σ quantum defects, respectively, reflect evolution from $3p$ and $4p$ united atom levels to O($3s$) and H($2s$) levels in the separated atom, respectively.

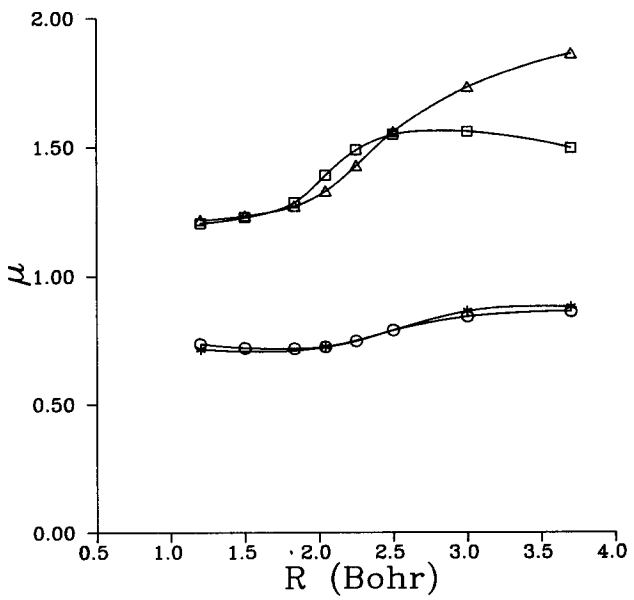

FIG. 3. Calculated quantum defect functions for OH $^2\Sigma^-$ ($1\pi^2 n\sigma, n = 4$–7) Rydberg states. 4σ—triangle; 5σ—circle; 6σ—square; 7σ—star.

4. Rate of Rydbergization and orbital evolution

In OH, as for several other first-row hydrides (e.g., BH, CH, and NH[50,51]), the $3s\sigma$ Rydberg orbital is penetrating to the extent that there is very strong mixing with the localized antibonding orbital $2p_O - 1s_H$. From Eq. (5), the first (repulsive) Rydberg state of Σ symmetry ($\alpha = 1$) is therefore represented approximately as

$$\Psi_{\alpha=1,\sigma} \simeq C_{1\sigma}^{\alpha=1}|\Phi_{\text{core}}(\phi_{2p_O} - \phi_{H_{1s}})| + C_{2\sigma}^{\alpha=1}|\Phi_{\text{core}}\phi_{3s}|.$$

In OH, this state correlates with the fluorine $3s$ level at $R = 0$ (see Fig. 2). The process of conversion from a valence orbital representation to Rydberg at smaller internuclear distances was termed "Rydbergization" by Mulliken.[51] Mulliken[51] pointed out that Rydbergization of the first orbital would proceed at different rates in different but related molecular states. The rate of Rydbergization of orbital form associated with the first repulsive state, as well as evolution of the higher bound Rydberg orbitals, is quantitatively reflected in our partial-wave decompositions in Table I, or equivalently as linear combinations of the coefficients $C_{n\sigma}^{\alpha}$ of Eq. (5). Note specifically that the Rydberg orbitals evolve with R at a rate approximately *twice* that of the antibonding 4σ level beyond $\sim 2a_0$. The 4σ orbital rapidly stabilizes to the $2p_O$ and $1s_H$ orbitals, while the Rydberg levels interact with other members (at the one-electron level) and pseudocross throughout the range between ~ 2–$3.5a_0$. This rate of orbital change is also qualitatively indicated in the quantum defect functions as R increases (Fig. 3).

The asymmetric nature of the electronic charge distribution as light hydrides dissociate significantly influences the rate of orbital evolution, as compared with H_2. At $R = 3.5a_0$, the Rydberg orbitals of H_2 with the same electronic Σ symmetry and excitation level as considered here have nearly united atom character.[49] Compared with H_2 Rydberg states, the Rydberg orbitals of the asymmetric case appear to evolve much more rapidly towards the separated atoms. This circumstance is obviously important for any photoabsorption or photoionization process via these states. This remark is supported by the previous discussion and can be understood further by the following considerations: First, the amplitude of the excited electron must become associated with one of two *distinguishible* nuclei at dissociation. This is a simplifing circumstance in comparison with homonuclear diatomics, since even a minimal description of their wave functions at large R must be represented as combinations of singly and doubly excited configurations to correctly represent dissociation. Second, we may estimate from the elementary Slater rule's[52] the effective charge on the core experienced by an electron in a $3s$ or $3p$ Rydberg orbit to be

$Z^* \sim +1.75$. Let $Z^* = Z_{\text{ion}} + Z_{\text{residual}}$. Since $Z_{\text{ion}} = +1$ and the Rydberg electron has nearly unit negative charge outside the core, a "hole" with charge $Z_{\text{residual}} \sim +0.75$ must reside primarily about one distinguishible nuclear center. Therefore, even with extensive screening by core electrons about the nucleus of higher Z, a Rydberg orbital with mean dimensions *larger* than the internuclear separation will sense a relatively localized hole at moderate internuclear distances.

B. Fixed-nuclei quantities

1. $D\,^2\Sigma^-(1\pi^2 3p\sigma)$ Rydberg state

In Figs. 4 and 5, we show our fixed-nuclei cross sections for ionization from the $D\,^2\Sigma^-$ Rydberg state, for the $5\sigma \rightarrow k\sigma$ and $5\sigma \rightarrow k\pi$ channels. The $k\pi$ cross sections were discussed in Ref. 13; however, we include them here for completeness and further discussion and analysis of the Cooper minimum in this channel. Focusing on the $k\pi$ channel of Fig. 4(b), we see that at small R the cross section is significantly depressed

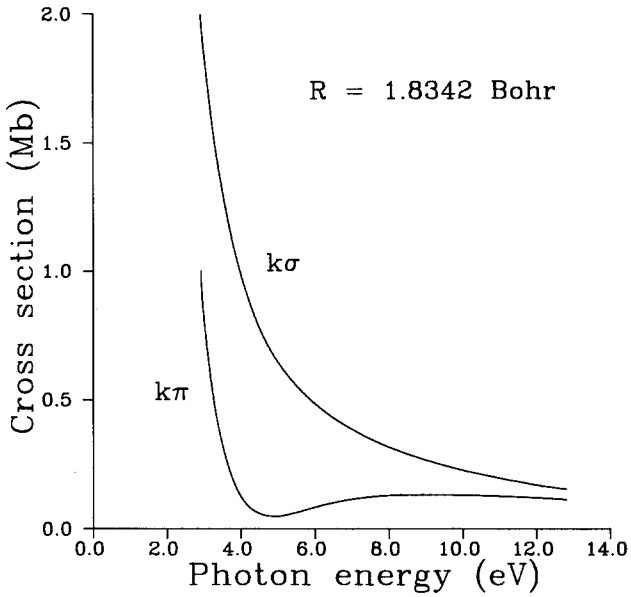

FIG. 5. Calculated (velocity form) photoionization cross sections for the $5\sigma \rightarrow k\pi$ channels at small internuclear distance. The cross sections assume an ionization potential of 2.81 eV. The Cooper minimum is not apparent in the total cross section.

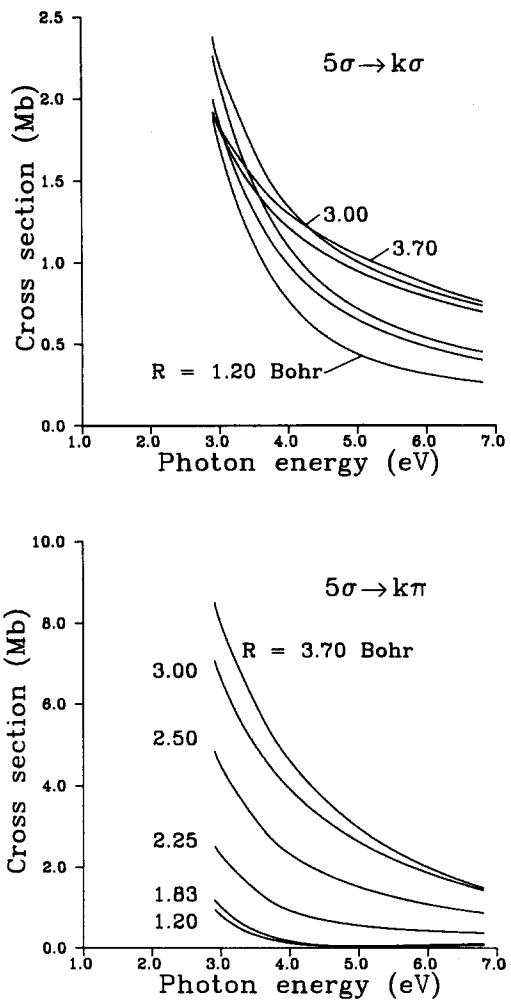

FIG. 4. Calculated (velocity form) photoionization cross sections for the $5\sigma \rightarrow k\sigma$ and $5\sigma \rightarrow k\pi$ channels at various internuclear distances. The cross sections assume an ionization potential of 2.81 eV.

over a rather large energy range, owing to a "$3p \rightarrow kd$" atomiclike Cooper minimum in this channel. As R increases, the 5σ orbital evolves into mainly one of O($3s$) character, as discussed in the previous section. This state is more spatially diffuse, allowing greater overlap with the photoelectron wave function, which in turn results in a large increase in the cross section at large R. Additionally, the $3s$ radial wave function has two nodes which disfavors a simple cancellation in the radial matrix element which occurs in the $3p$ (one node) case. We have not found a Cooper minimum at any energy at these larger internuclear distances, although possibly one occurs below threshold in the discrete. Note that the variation of the cross section is weak at small $R(\sim 1.2\text{–}1.8a_0)$ or large $R(\sim 3.0\text{–}3.7a_0)$ due to the rather slow evolution of the Rydberg orbital in these ranges.

In Fig. 4, the $5\sigma \rightarrow k\sigma$ cross sections show relatively weak variation with internuclear distance. (Note the different ordinate scales in Fig. 4.) In particular, no Cooper minimum is evident in this channel. This is a consequence of greater penetration of the $k\sigma$ orbital into the molecular interior (which also has its orientation along the molecular axis) and subsequent greater l mixing among its components from the anisotropic molecular-ion field. In Fig. 5, we show on a different scale the $k\pi$ and $k\sigma$ cross sections at the internuclear distance $R = 1.8342a_0$, which displays the spectral range of the Cooper minimum in comparison with the $k\sigma$ channel. This illustrates that even with tuning of the ionizing photon in a $(2+1)$ or $(3+1)$ two-color REMPI experiment, the influence of the Cooper minimum is likely to be of consequence over a rather wide spectral range.

To observe sign changes in dipole amplitudes associated with Cooper minima in molecules, it is most appropriate to examine the real, principal-part (standing-wave normalized) dipole amplitudes given by[53]

$$D^P_{lmm'} = \sum_{l'l''} \left\langle \frac{\phi_{l'm'}(r)}{r} Y_{l'm'}(\hat{r}) | O_\mu | \frac{\psi^P_{l''lm}(r)}{r} Y_{l''m}(\hat{r}) \right\rangle, \quad (7)$$

where $\phi_{l'm'}(r)$ is a partial-wave component of the bound-state wave function given in Eq. (3a), $\psi^P_{l''lm}(r)$ is a partial-wave component of the photoelectron radial wave function, and O_μ is the length or velocity form dipole operator [see Eq. (2)]. The integration over the angular and radial variables results in

$$D^P_{lmm'} = \sum_{l'l''} C(l',l'',m',m,\mu) \int_0^\infty dr\, \phi^*_{l'm'}(r) O_\mu(r) \times \psi^P_{l''lm}(r), \quad (8)$$

where the angular factor $C(l',l'',m',m,\mu)$ is given by Eq. (68) of Ref. 53. It is restricted to nonzero values for projections $m' = \mu + m$ and for orbital momenta $l' + l'' + 1 = even$, and $|l'' - 1| \leqslant l' \leqslant l'' + 1$.

In Fig. 6, we show our dipole amplitudes $D^P_{lmm'}$ for $l = 1$–3 components of the $5\sigma \rightarrow k\pi$ channel at $R = 1.8342a_0$. The dominance of the $l = 2$ component, noted earlier,[13] clearly defines the Cooper minimum in this channel. Since l is not a good quantum number in a molecule, however, Cooper minima may appear in more than one asymptotic channel l, the label on the left-hand side of Eqs. (8) and (9). This can be seen in Fig. 3 of Ref. 13, where we plotted the incoming-wave normalized amplitudes $|D^{(-)}_l|^2$ and in Fig. 6 for the real amplitudes. Interestingly, the sign changes and minima occur in the $l = 2$ and 3 component at the *same* photoelectron kinetic energy. There is also a weak-minimum in the $l = 1$ component, which is more apparent in the renormalized amplitudes discussed in Ref. 13. This can be explained as follows: For photoionization of the $D\,^2\Sigma^-$ state, there are only a limited number of partial waves which are physically relevant in Eq. (8). At $R = 1.8342a_0$, the 5σ orbital is composed of $l' = 0$ and 1 waves, with the latter waves dominant since it is a $3p$-type Rydberg orbital at this R. For the $k\pi$ continuum, only the $l = 1$–3 waves are important. The projection quantum numbers are $m' = 0$, $m = 1$, and $\mu = -1$. With these parameters, to a good approximation, only two terms survive for each l, giving

$$D^P_{l10} \simeq -\frac{1}{\sqrt{3}} \int_0^\infty dr\, \phi_{00}(r) O_{-1}(r) \psi^P_{l1}(r) - \frac{1}{\sqrt{5}} \int_0^\infty dr\, \phi_{10}(r) O_{-1}(r) \psi^P_{2l1}(r), \quad (9)$$

where the coefficients $-1/\sqrt{3}$ and $-1/\sqrt{5}$ are the angular factors. The radial matrix elements in Eq. (9) indicate that in the inner region (body frame) of the molecule, the $0 \rightarrow 1$ and $1 \rightarrow 2$ transitions are dominant for *all* l. That is, even for an asymptotic f wave ($l = 3$), the $l = 2$ wave of the final state contributes to the dipole amplitude in regions of the molecule extending from $\sim$0–$10a_0$, where overlaps and thus cancellations in the radial matrix element may occur. Thus, the minimum in the $l = 3$ amplitude remains a consequence of the $3p \rightarrow kd$ Cooper minimum prominent at smaller internuclear distances. The smaller magnitude of D^P_{310} reflects both the inability of the f wave to penetrate into the molecular interior at low kinetic energy, and relatively weak rescattering from initial d-wave photoejection. The $l = 1$ component does not show a sign change, due to its primary contribution arising from the "3s"-wave radial function with two nodes, which prevents simple cancellation in this energy range.

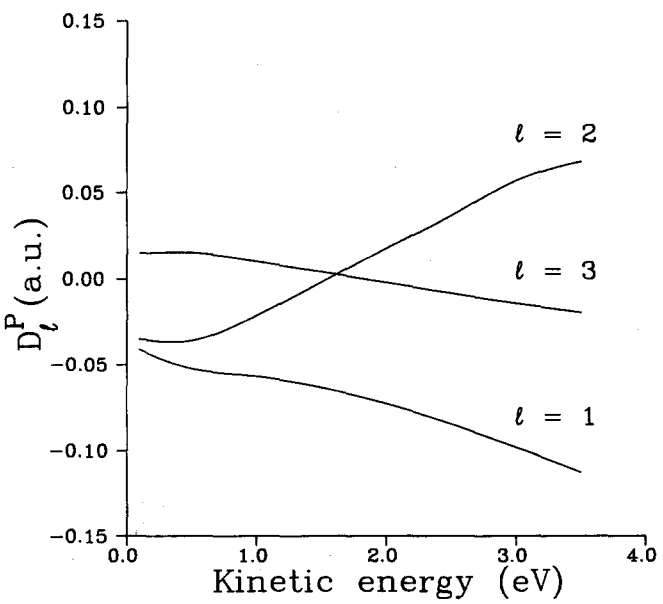

FIG. 6. Calculated real dipole amplitudes (standing-wave normalized, velocity form) for the $5\sigma \rightarrow k\pi$ channel, $l = 1$–3 continuum partial waves, at $R = 1.8342\ a_0$.

2. $3\,^2\Sigma^-(1\pi^2 4s\sigma)$ Rydberg state

In Fig. 7, we show our fixed-nuclei cross sections for ionization from the $3\,^2\Sigma^-$ Rydberg state for the $k\sigma$ and $k\pi$ ionization channels. Note that the effective variation of the cross sections with R is weaker than that seen for the $D\,^2\Sigma^-$ state, for two reasons. First, the normalization factor of a Rydberg state is proportional to $1/n^{*3/2}$, where n^* is the effective quantum number. Since this increases by one unit for the 4s level, the photoelectron matrix elements accordingly decrease approximately by this factor. Second, at smaller internuclear distances, the Rydberg orbital is of 4s type and the extra radial node compared to a $3p$ Rydberg function diminishes a simple cancellation in the matrix element as the kinetic energy varies. The Cooper minima for the $6\sigma \rightarrow k\sigma, k\pi$ channels are apparent only at quite small kinetic energy and are revealed only upon analysis of partial-wave components of the dipole strength. In Fig. 8, we show contributions to the dipole strength $\Sigma_l |D^{(-)}_l|^2$ for the $6\sigma \rightarrow k\pi$ and $6\sigma \rightarrow k\sigma$ channels at the internuclear distances $R = 1.20$ and $3.70a_0$. A similar analysis at small R was discussed for the $5\sigma \rightarrow k\pi$ channel in Ref. 13. In Fig. 8, some of the partial-wave dipole matrix elements show weak Cooper minima. These may in general extend across threshold, or even be apparent only in the adjoining discrete.[23] At $R = 1.20a_0$, the $4s\sigma$ wave function is strongly mixed with the $4p\sigma$ level,

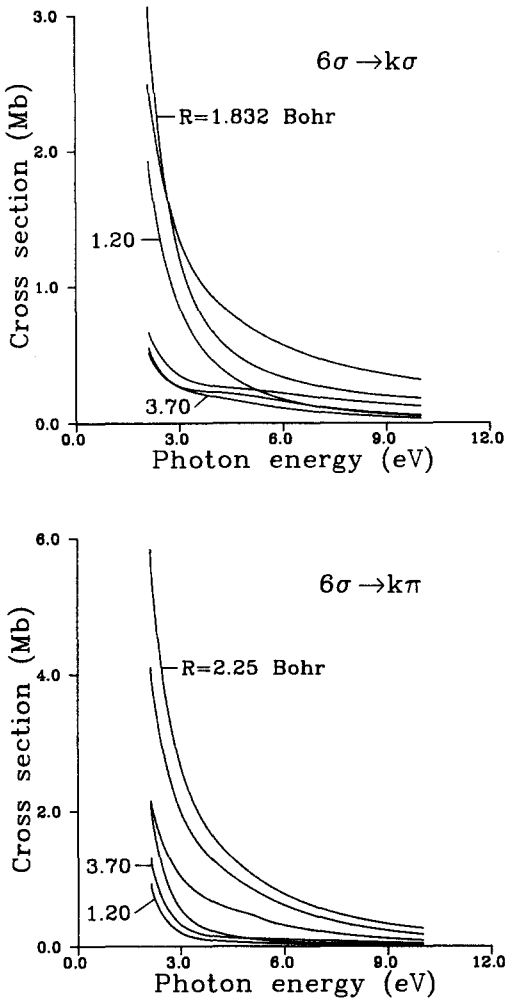

FIG. 7. Calculated (velocity form) photoionization cross sections for the $6\sigma \rightarrow k\sigma$ and $6\sigma \rightarrow k\pi$ channels at various internuclear distances. The cross sections assume an ionization potential of 2.81 eV.

which accounts for the strong $l = 0$ contribution to the total dipole strength. At large R [Fig. 8(b)], the Rydberg wave function is strongly mixed among the hydrogen $2s$ and oxygen $3p$ levels, as discussed in Sec. III. The d-wave Cooper minimum which extends into the discrete spectra arises from transition from the oxygen $3p$ orbital which mixes with the 6σ orbital at large R. In Fig. 8, Cooper minima in the partial-wave dipole amplitudes for the $6\sigma \rightarrow k\pi$ channel are more apparent than the $6\sigma \rightarrow k\sigma$ channel, although they are weaker than the corresponding $5\sigma \rightarrow k\pi$ transition. The prominent $4s \rightarrow kp$ Cooper minima at $R = 1.20$ is masked in the total dipole strength by the $4p \rightarrow kd$ amplitude. At large R, the weak Cooper minimum in the total dipole strength arises from the oxygen $3p \rightarrow kd$ transition as well as other partial-wave components, a consequence of the greater l mixing at large R and higher levels of Rydberg excitation.

C. Vibrational branching ratios and photoelectron angular distributions

In Figs. 9–13, we show our calculated vibrationally resolved branching ratios and photoelectron angular distributions for the 5σ and 6σ Rydberg states of OH for $(3+1)$ REMPI via these states. The 5σ branching ratios were previously discussed.[13] We have replotted them here for comparison with the 6σ results and with an alternative normalization, such that a sum over accessible ion vibrational levels equals unity.[54] The non-Franck–Condon effects apparent in the 5σ branching ratios in Fig. 9 arises from the combined effect of rapid change of the Rydberg orbital with R (particularly at intermediate to larger internuclear distances) and a Cooper minimum occurring at small R, where the energy levels correspond closely to the united atom levels (see Figs. 1 and 2).

In Fig. 10, we show our calculated branching ratios for the 6σ Rydberg state. In this calculation, we employed the potential energy curve of van Dishoeck *et al.*[15], which when interpolated gives an equilibrium internuclear distance value of $R_e = 2.16a_0$. In Fig. 10, the broad vibrational distributions conform rather well with the Franck–Condon predictions, with minimal deviations due to R dependence of the transition moment induced by the orbital evolution.

In Fig. 11, we show calculated branching ratios for the 6σ Rydberg state, employing our calculated IVO potential energy curve, which gives $R_e = 1.97a_0$ and is rather close to the $X^3\Sigma^-$ ion value of $R_e = 1.94a_0$. Note that the vibrational distributions are strongly peaked in the $\Delta v = 0$ transition with some apparent deviation from Franck–Condon predictions for off-diagonal transitions. The maximum intensity predicted for the $\Delta v \neq 0$ transition is 18%–20% in the $\Delta v = 1$ channel, in contrast to the nearly 40% intensity predicted for the 5σ level. This diminished non-Franck–Condon effect in the 6σ level is due to the inherent weaker dependence of the dipole transition moment on R, which in turn derives from the nature of the orbital evolution at higher Rydberg excitation, as discussed in Sec. III. In the absence of perturbations of the intermediate level and final-state effects which can lead to non-Franck–Condon vibrational distributions in REMPI (such as shape resonances and electronic autoionization),[5–13] one may generally expect greater adherence to Franck–Condon factorization of the transition moment, which will result in better vibrational state selection in the hydride ion produced. The large difference between Figs. 10 and 11 reflects the considerable uncertainty ($\sim \pm 0.1a_0$) in the R_e values for this state, which changes the Franck–Condon distribution itself.[55]

Figures 12 and 13 present vibrationally resolved photoelectron angular distributions for the $D^2\Sigma^-$ and $3^2\Sigma^-$ Rydberg states. The angular distributions in these figures have been plotted in the usual manner, i.e., for an unaligned molecular target, we have the distribution

$$\frac{d\sigma}{d\omega} \propto 1 + \beta P_2(\cos\theta), \tag{10}$$

where β is the asymmetry parameter, θ is the angle between the direction of the light polarization and the photoelectron momentum, and P_2 is a Legendre polynomial. Studies of rotationally resolved REMPI of OH and other diatomic hydrides, which include alignment effects induced by the multiphoton absorption process, have been completed.[56,57] In Fig. 12, the angular distributions depend on the final vibra-

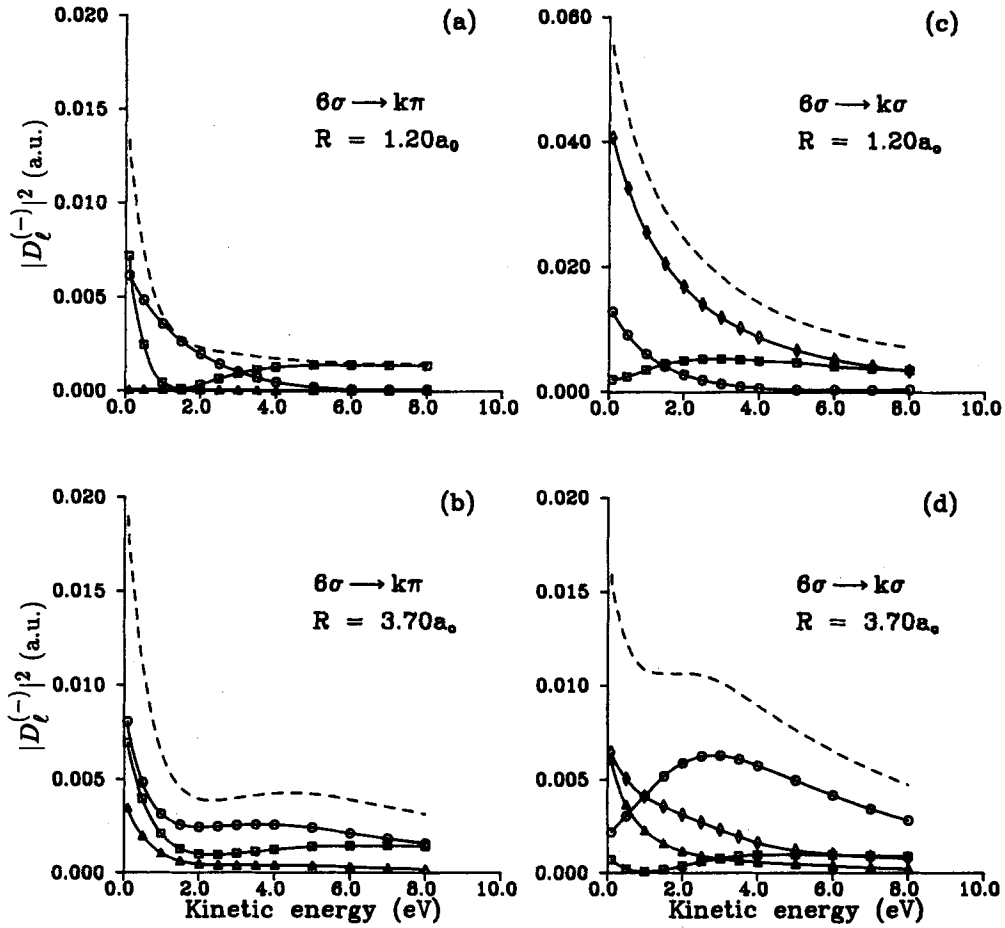

FIG. 8. Calculated dipole strengths (incoming-wave normalized, velocity form) for (a) and (b), the $6\sigma \rightarrow k\pi$ channel: $l = 1$—square; $l = 2$—circle; $l = 3$—triangle; (c) and (d), $6\sigma \rightarrow k\sigma$ channel: $l = 0$—diamond; $l = 1$—square; $l = 2$—circle; $l = 3$—triangle. The dashed curve in each frame is the sum of partial-wave contributions.

tional state of the ion, further indicating the non-Franck–Condon effects induced by the orbital evolution, although the effect here is not as strong as induced by shape resonances.[5,8–13] Furthermore, as apparent in Fig. 12, the angular distribution is peaked towards $\theta = 90°$, reflecting an asymmetry parameter with a value approaching $\beta = -1$. In the angular distribution theory of Dill and Fano,[58] the angular momentum transfer between the initial state (molecule + photon) and final state (ion + photoelectron) is $\mathbf{j}_t = \mathbf{j}_\gamma - \mathbf{l}$, where $\mathbf{j}_\gamma$ is the angular momentum of the light and

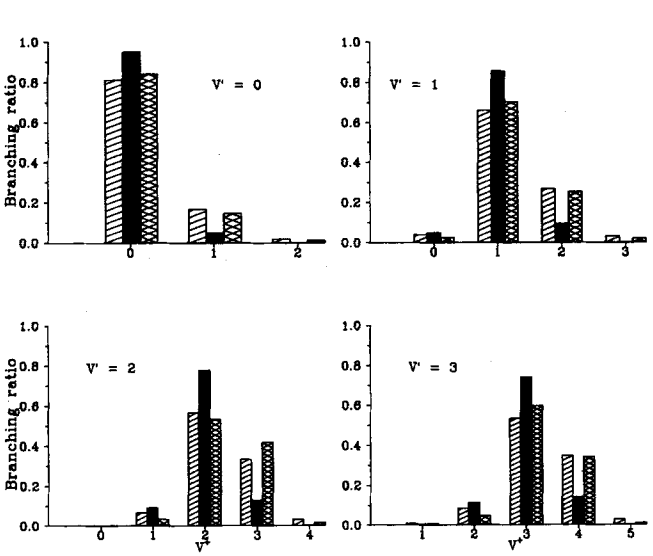

FIG. 9. Calculated vibrational branching ratios for OH $D\,^2\Sigma^-$ ($v' = 0$–3) photoionization. The one-photon energies for the $v' = 0$–3 frames, respectively, are 3.38, 3.48, 3.59, and 3.69 eV. Franck–Condon ratio (solid bar); full, length form (slashed bar); full, velocity form (cross-hatched bar).

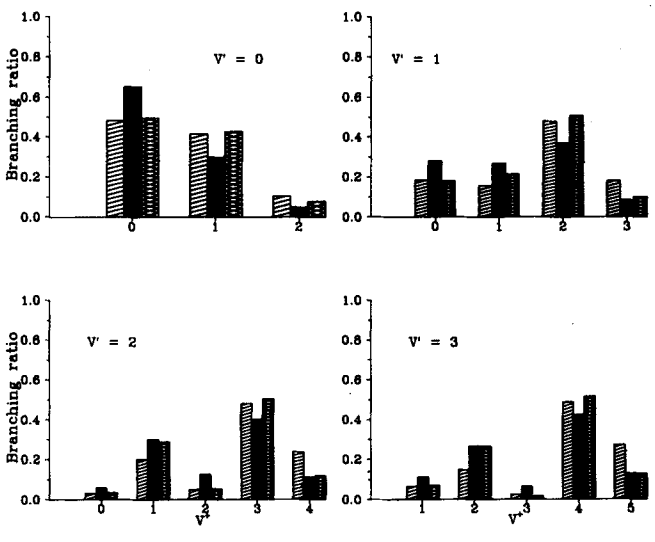

FIG. 10. Calculated vibrational branching ratios for OH $3\,^2\Sigma^-$ ($v' = 0$–3) photoionization using the Rydberg potential curve of Ref. 15 ($R_c = 2.16a_0$). The one-photon energies for the $v' = 0$–3 frames, respectively, are 3.67, 3.76, 3.86, and 3.95 eV. Franck–Condon ratio (solid bar); full, length form (slashed bar); full, velocity form (cross-hatched bar).

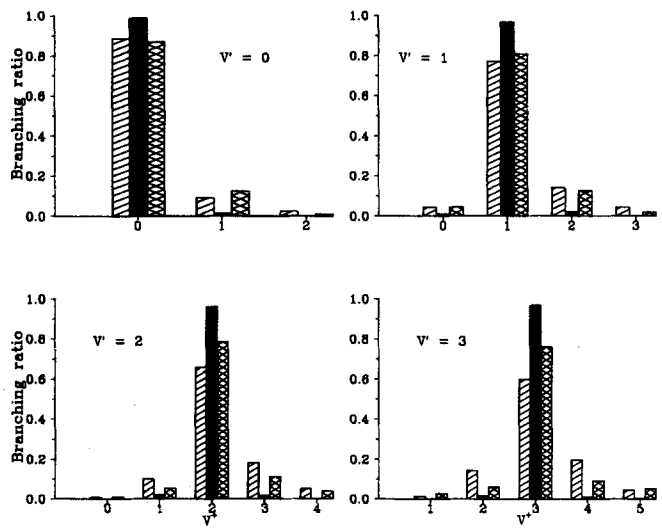

FIG. 11. Calculated vibrational branching ratios for OH $3\,^2\Sigma^-$ ($v' = 0$–3) photoionization using our IVO Rydberg potential curve ($R_e = 1.97a_0$). The one-photon energies for the $v' = 0$–3 frames, respectively, are 3.67, 3.78, 3.90, and 4.02 eV. Franck–Condon ratio (solid bar); full, length form (slashed bar); full, velocity form (cross-hatched bar).

l is the orbital angular momentum of the photoelectron. The contributions to β from angular momentum transfers $j_t = l$ result in $\beta(j_t) = -1$ exactly.[58] In Fig. 12, the peaking of the photocurrent which is largely orthogonal to the electric vector of the light **E** is due to parity-unfavored contributions in the $5\sigma \rightarrow k\pi$ channel with $^2\Sigma^-$ final-state symmetry. The $5\sigma \rightarrow k\sigma$ has a strong $l = 0$ component which cannot contrib-

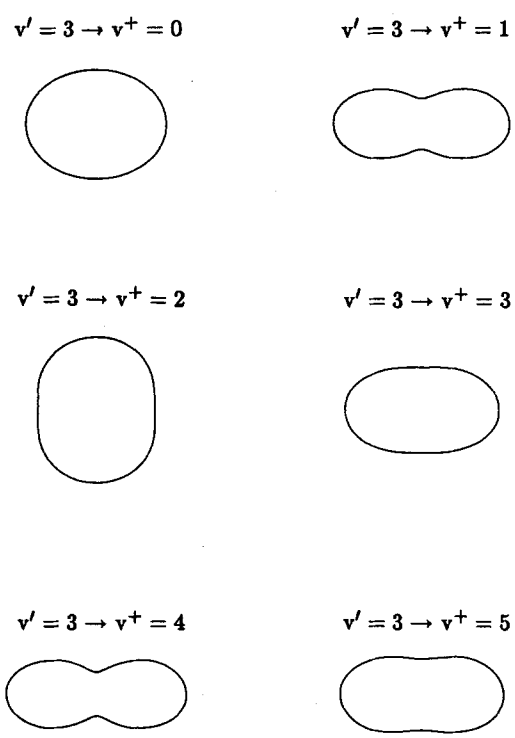

FIG. 12. Calculated vibrationally resolved photoelectron angular distributions (velocity form) for OH $D\,^2\Sigma^-$ ($v' = 3$) photoionization.

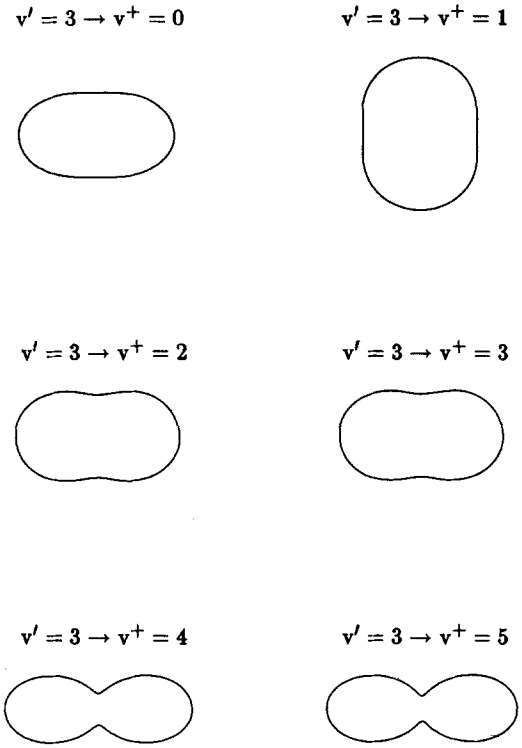

FIG. 13. Calculated vibrationally resolved photoelectron angular distributions (velocity form) for OH $3\,^2\Sigma^-$ ($v' = 3$) photoionization using the Rydberg potential energy curve of Ref. 15.

ute to parity-unfavored transitions. The non-Franck–Condon effect is most pronounced in the $k\pi$ channel, due to its R dependence, and this is reflected in the large weight of this channel in, e.g., the $v' = 3 \rightarrow v^+ = 4,5$ distributions. In Fig. 13, the overall non-Franck–Condon effect in the off-diagonal angular distributions is weaker compared with those in Fig. 12, for reasons discussed in Sec. III.

IV. CONCLUSION

In this paper, we have discussed and pointed out the relevance of rapid orbital evolution processes in the $^2\Sigma^-$ Rydberg states OH, which are applicable to other Rydberg states of the first row hydrides as well. The technique of REMPI coupled with high-resolution photoelectron spectroscopy offers a unique possibility to probe regions of the configuration space of the Rydberg electron where its orbital evolution rapidly proceeds towards the separated atom products. Our analysis shows that this occurs over a rather short range of internuclear distances in these systems, with important spectroscopic implications for both vibrationally and rotationally resolved REMPI spectroscopy via these Rydberg states. Although the study of continuum features such as shape resonances, autoionization, and Cooper minima phenomenon are of fundamental interest in atomic and molecular physics, for molecules there is practical interest in the preparation of quantum state-selected molecular ions. Vibrational state selection in the hydride fragments using REMPI techniques may be enhanced by photoionization of the higher-lying Rydberg states, since effects due to "clean" Cooper zeros in the threshold region may be minimized.

This is due to greater l mixing and a more complex nodal structure of the Rydberg wave functions, as well as a closer resemblance of the Rydberg potential to that of the ion core.

ACKNOWLEDGMENTS

We thank Dr. Helene Levebvre-Brion for pointing out Refs. 24 and 25 and for a helpful discussion and encouragement. One of us thanks Dr. Michael Cavagnero for pointing out Ref. 45 and a helpful discussion and Dr. K. T. Lu for a helpful discussion on quantum defect functions. Finally, we thank Dr. Ewine van Dishoeck for providing numerical values of the potential energy curves from her publications. This work was supported by grants from the National Science Foundation (CHE-8521391), Air Force Office of Scientific Research (Contract No. 87-0039), and the Office of Health and Environmental Research of the U. S. Department of Energy (DE-FG03-87ER60513). We also acknowledge use of resources of the San Diego SuperComputer Center, which is supported by the National Science Foundation.

[1] R. N. Compton and J. C. Miller, in *Laser Applications in Physical Chemistry*, edited by D. K. Evans (Dekker, New York, 1988), Sec. 4.
[2] P. M. Dehmer, J. L. Dehmer, and S. T. Pratt, Comments At. Mol. Phys. **19**, 205 (1987).
[3] K. Kimura, Adv. Chem. Phys. **60**, 161 (1985).
[4] J. P. Reilly, Israel J. Chem. **24**, 266 (1984).
[5] W. A. Chupka, J. Chem. Phys. **87**, 1488 (1987).
[6] A. P. Hickman, Phys. Rev. Lett. **59**, 1553 (1987).
[7] S. N. Dixit, D. L. Lynch, V. McKoy, and A. U. Hazi, Phys. Rev. A **40**, 1700 (1989).
[8] P. J. Miller, L. Li, W. A. Chupka, and S. D. Colson, J. Chem. Phys. **89**, 3921 (1988).
[9] J. A. Stephens, M. Braunstein, and V. McKoy, J. Chem. Phys. **89**, 3923 (1988).
[10] P. J. Miller, W. A. Chupka, J. Winniczek, and M. G. White, J. Chem. Phys. **89**, 4058 (1988).
[11] M. Braunstein, J. A. Stephens, and V. McKoy, J. Chem. Phys. **90**, 633 (1989).
[12] J. A. Stephens, M. Braunstein, and V. McKoy, J. Chem. Phys. **92**, 5319 (1990).
[13] J. A. Stephens and V. McKoy, Phys. Rev. Lett. **62**, 889 (1989).
[14] E. F. van Dishoeck, S. R. Langhoff, and A. Dalgarno, J. Chem. Phys. **78**, 4552 (1983).
[15] E. F. van Dishoeck and A. Dalgarno, J. Chem. Phys. **79**, 873 (1983).
[16] D. R. Bates, Mon. Not. R. Astron. Soc. **106**, 432 (1946). For early experimental results, see the paper of R. W. Ditchburn, J. Tunstead, and J. G. Yates, Proc. R. Soc. London Ser. A **181**, 386 (1943).
[17] M. J. Seaton, Proc. R. Soc. London Ser. A **208**, 418 (1951).
[18] J. W. Cooper, Phys. Rev. **128**, 681 (1962).
[19] U. Fano and J. W. Cooper, Rev. Mod. Phys. **40**, 441 (1968).
[20] T. A. Carlson, M. O. Krause, W. A. Svensson, P. Gerard, F. A. Grimm, T. A. Whitley, and B. P. Pullen, Z. Phys. D **2**, 309 (1986).
[21] S. T. Manson, Phys. Rev. A **31**, 3968 (1985).
[22] A. Msezane and S. T. Manson, Phys. Rev. Lett. **35**, 364 (1975); **48**, 473 (1982); J. Lahiri and S. T. Manson, *ibid.* **48**, 614 (1982).
[23] S. Fredin, D. Gauyacq, M. Horani, C. Jungen, G. Lefevre, and F. Masnou-Seeuws, Mol. Phys. **60**, 825 (1987).
[24] F. Masnou-Seeuws and Ch. Jungen, in *Proceedings of the XIV International Conference on the Physics of Electronic and Atomic Collisions*, edited by P. J. Coggiola, D. L. Huestis, and R. P. Saxon (North Holland, Palo Alto, 1985), p. 83.
[25] P. Labastie, M. C. Bordas, B. Tribollet, and M. Broyer, Phys. Rev. Lett. **52**, 1681 (1984).
[26] K. Wang, J. A. Stephens, and V. McKoy, J. Chem. Phys. **93**, 7874 (1990).
[27] H. Rudolph, J. A. Stephens, V. McKoy, and M. T. Lee, J. Chem. Phys. **91**, 1374 (1989).
[28] H. Rudolph and V. McKoy, J. Chem. Phys. **91**, 7995 (1989).
[29] H. Rudolph and V. McKoy, J. Chem. Phys. (accepted for publication).
[30] R. R. Lucchese and V. McKoy, J. Phys. B **14**, 1629 (1981).
[31] P. M. Dittman, D. Dill, and J. L. Dehmer, J. Chem. Phys. **76**, 5703 (1982).
[32] G. Raseev, H. Le Rouzo, and H. Lefebvre-Brion, J. Chem. Phys. **72**, 5701 (1980).
[33] R. R. Lucchese, G. Raseev, and V. McKoy, Phys. Rev. A **25**, 2572 (1982).
[34] R. R. Lucchese, K. Takatsuka, and V. McKoy, Phys. Rep. **131**, 147 (1986).
[35] W. J. Hunt and W. A. Goddard, Chem. Phys. Lett. **3**, 414 (1967).
[36] J. A. Stephens and V. McKoy, J. Chem. Phys. **88**, 1737 (1988).
[37] H.-J. Werner, P. Rosmus, and E.-A. Reinsch, J. Chem. Phys. **79**, 905 (1983).
[38] H. Lefebvre-Brion, C. M. Moser, and R. K. Nesbet, J. Mol. Spectrosc. **13**, 418 (1964); H. Lefebvre-Brion, J. Mol. Struc. **19**, 103 (1973); H. Lefebvre-Brion, J. de Phisique (colloque C5a, supplement no. 10) **32**, 107 (1971). The last two papers report the first calculations on the $1\,^2\Sigma^-$, $D\,^2\Sigma^-$, and $3\,^2\Sigma^-$ Rydberg states of OH using the IVO procedure. The total energies and energy differences relative to the ground state are in good agreement with the present calculations.
[39] V. Sidis and H. Lefebvre-Brion, J. Phys. B **4**, 1040 (1971).
[40] M. Rajzmann, F. Spiegelmann, and J. P. Malrieu, J. Chem. Phys. **89**, 433 (1988).
[41] W. Weizel, in *Handbuch der Experimentalphysik*, edited by W. Wein and F. Harms (Akademische, Leipzig, 1931), Vol. 1, p. 42.
[42] R. S. Mulliken, Rev. Mod. Phys. **4**, 1 (1932).
[43] P. M. Morse and E. Stückelberg, Phys. Rev. **33**, 211 (1972).
[44] S. S. Gershtein and V. D. Krivchenkov, Sov. Phys. JETP **13**, 1044 (1961).
[45] M. Barat and W. Lichten, Phys. Rev. A **6**, 211 (1972).
[46] A. E. Douglas, Can. J. Phys. **52**, 318 (1974).
[47] C. E. Moore, *Atomic Energy Levels, as Derived from the Analyses of Optical Spectra*, (U. S. Government Printing Office, Washington, D. C., 1971), Vol. 1, pp. 60–61.
[48] G. Herzberg, *Spectra of Diatomic Molecules* (Van Nostrand, New York, 1950), Chap. 6.
[49] Ch. Jungen and O. Atabek, J. Chem. Phys. **66**, 5584 (1977).
[50] H. Lefebvre-Brion and R. W. Field, in *Perturbations in the Spectra of Diatomic Molecules* (Academic, Orlando, 1986), Chap. 4, Sec. 2.
[51] R. S. Mulliken, Acc. Chem. Res. **9**, 7 (1976); Chem. Phys. Lett. **14**, 141 (1972); J. Am. Chem. Soc. **91**, 4615 (1969).
[52] P. W. Atkins, *Molecular Quantum Mechanics* (Clarendon, Oxford, 1970), Vol. 2, p. 262.
[53] R. R. Lucchese and V. McKoy, Phys. Rev. A **21**, 112 (1980).
[54] The single photon energies used for the $(3+1)$ calculations given in Ref. 13 were slightly incorrect, due to an incorrect choice of T_0. The resulting changes in the calculated branching ratios are negligible on the scale of Fig. 4 of Ref. 13 and Fig. 9 of this paper.
[55] At the time of completion of this manuscript, H. Wang and W. A. Chupka (Yale University) and E. De Beer, M. P. Koopmans, and C. A. deLange (University of Amsterdam) have measured $R_e = 2.07\ a_0$ for the $3\,^2\Sigma^-$ Rydberg state of OH, which lies between our two limits.
[56] K. Wang and V. McKoy (to be published).
[57] K. Wang, J. A. Stephens, H. Rudolph, and V. McKoy (to be published).
[58] D. Dill and U. Fano, Phys. Rev. Lett. **29**, 1203 (1972); D. Dill, Phys. Rev. A **6**, 160 (1972); U. Fano and D. Dill, *ibid.* **6**, 185 (1972).